Supplementary Information: "The recent enhancement of the surface melt over the Antarctic Peninsula dictated by thermodynamics "

Qinglin Zhang[1,2], Baojuan Huai[3], Sai Wang[1], Brice Noël[4], Michiel R. van den Broeke[5], Xavier Fettweis[4], Christoph Kittel[4,6], Dahe Qin[1], Minghu Ding[1,2]*

1. *State Key Laboratory of Disaster Weather Science and Technology, Chinese Academy of Meteorological Sciences, Beijing, China*
2. *Department of Atmospheric and Oceanic Sciences & Institute of Atmospheric Sciences & Key Laboratory of Polar Atmosphere-Ocean-Ice System for Weather and Climate, Ministry of Education, Fudan University, Shanghai*
3. *College of Geography and Environment, Shandong Normal University, Jinan, China*
4. *Laboratory of Climatology, Department of Geography, SPHERES research unit, University of Liège, Liège, Belgium*
5. *Institute for Marine and Atmospheric Research Utrecht, Utrecht University, Utrecht, Netherlands*
6. *Physical Geography Research Group, Department of Geography, Vrije Universiteit Brussel, Brussels, Belgium*

Corresponding author: Minghu Ding (dingminghu@foxmail.com)

This document includes:

- **Supplementary Figures 1-16**
- **Supplementary Table 1**
- **Supplementary Methods**
- **Supplementary References**

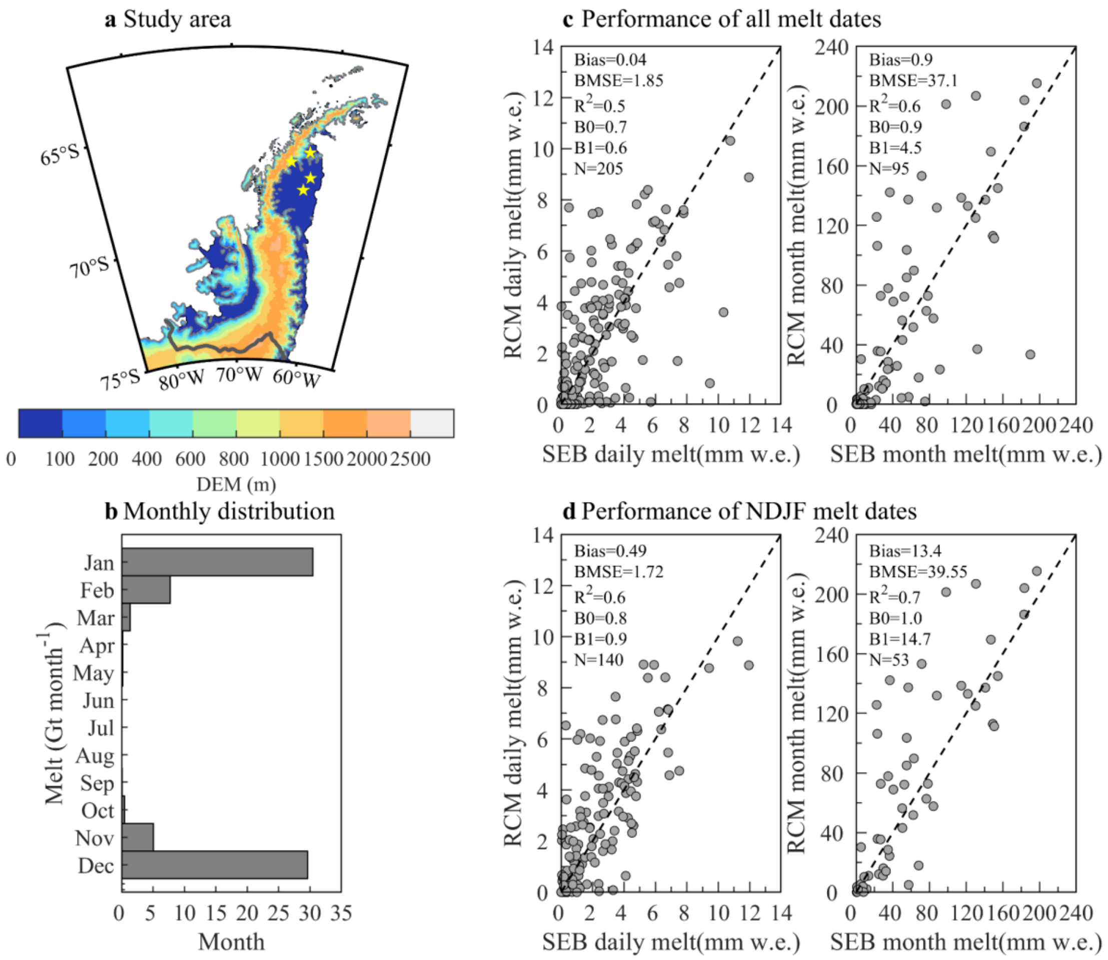

Supplementary Figure 1: Study area and the performance of RACMO2.3p2 of AP surface melt. **a** Study area and the distribution of AWSs used to force surface energy balance (SEB) model. **b** Monthly distribution of AP surface melt in RACMO2.3p2. **c** and **d** Performance of all dates' and NDJF surface melt rates from RACMO2.3p2, respectively. Shading in **a** indicate the altitude in model and yellow stars represent automatic weather stations used in the SEB model. The bold black line indicates the extent of the AP. Statistics in **c** and **d** show the number of data points (N), mean bias (Bias), root mean squared error (RMSE), correlation coefficient (R^2), regression slope (B0) and intercept (B1).

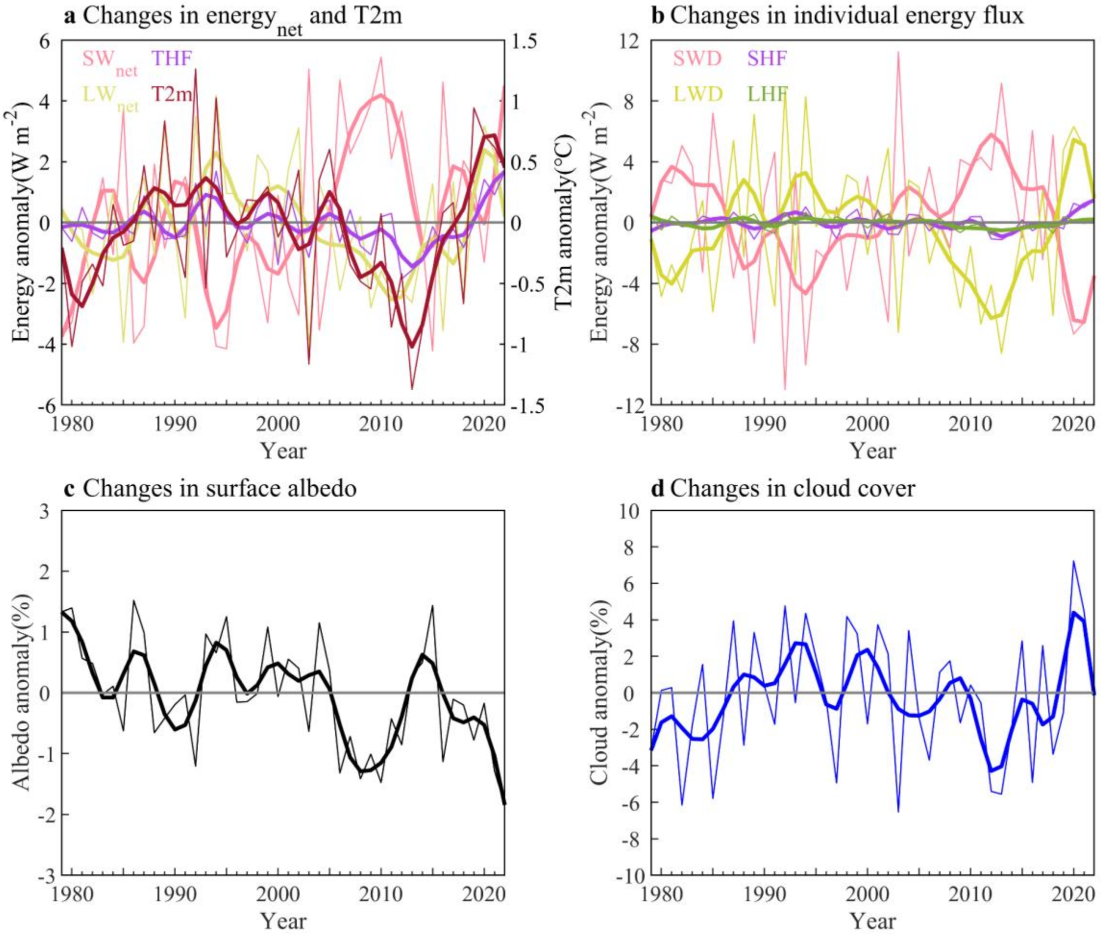

Supplementary Figure 2: Changes in NDJF average surface energy heat flux, air temperature, albedo and cloud anomalies in AP. **a** Time series of NDJF surface net shortwave radiation (SW_{net}), net longwave radiation (LW_{net}), turbulent heat fluxes (THF) and 2 m air temperature (T2m) anomalies from 1979 to 2022, relative to the 1979–2022 NDJF calendar daily mean. The bold lines represent the results after the five-year low-pass Butterworth filtering. **b** Same as **a** but for downward shortwave radiation (SWD), downward longwave radiation (LWD), sensible heat flux (SHF) and latent heat flux (LHF). (**c**, **d**), same as **a** but for surface albedo and average total cloud cover. All data in (**a**-**c**) come from RACMO. The albedo is computed based on SW_{net} and SWD. The cloud cover data is from ERA5.

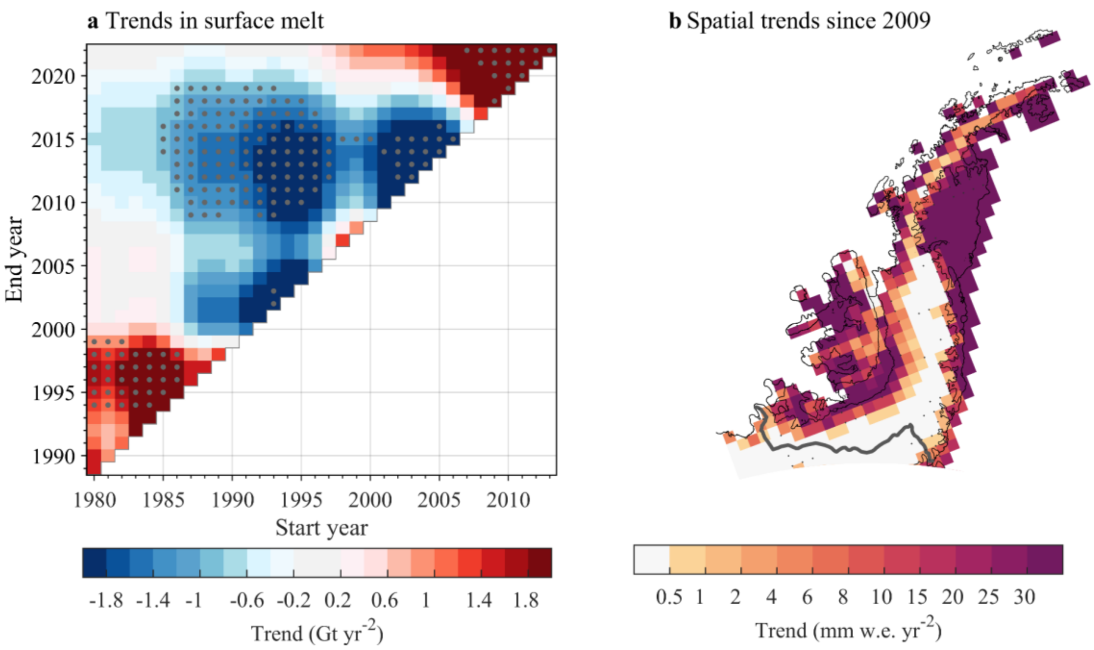

Supplementary Figure 3: Changes in AP NDJF surface melt from MAR v3.12. **a** Trends of AP surface melt in NDJF during different periods. Linear trends were computed based on the time series of NDJF surface melt after the five-year low-pass filtering. **b** Spatial distribution of NDJF linear trends since 2009. The grey dots in **a** and **b** represent the trends passing the (Hamed-Rao modified) Mann-Kendall significance test of the confidence level of 95%.

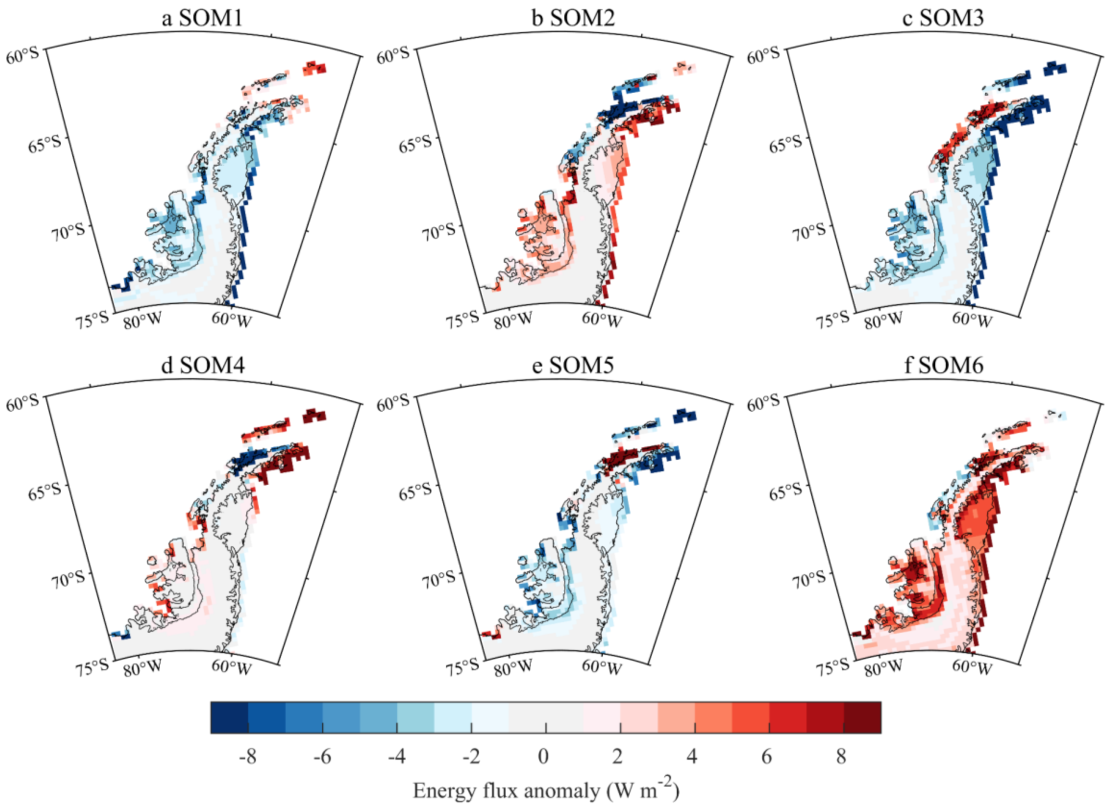

Supplementary Figure 4: Surface energy anomaly under each pattern. Shading in maps represents daily surface energy anomalies (SW_{net}+LW_{net}+SHF+LHF) relative to the average calendar daily melt during the NDJF period spanning from 1979 to 2022.

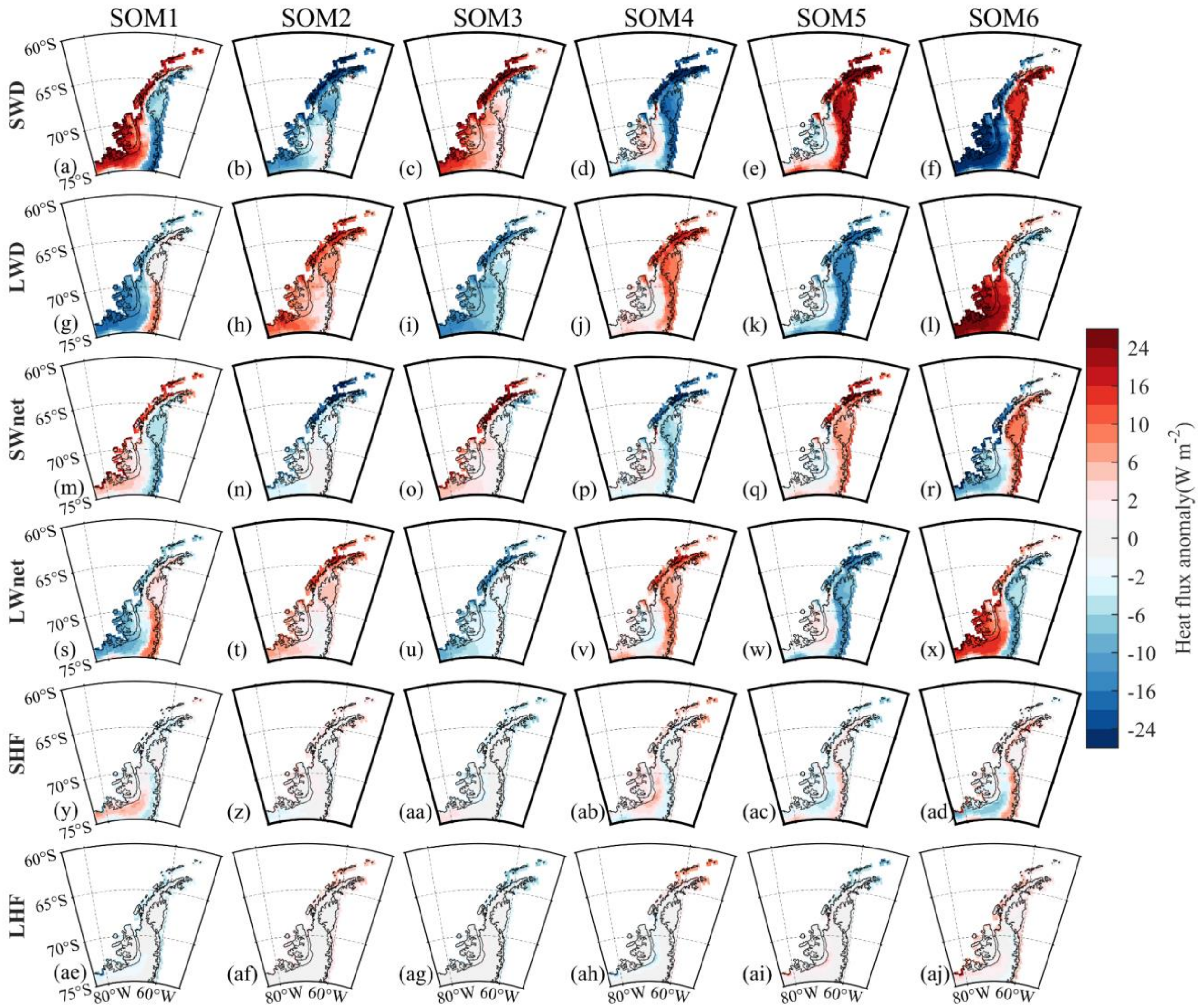

Supplementary Figure 5: Average energy anomalies during each circulation pattern in 1979-2022 NDJF. Energy anomalies from RACMO include downward shortwave radiation (SWD), downward longwave radiation (LWD), net shortwave radiation (SW_{net}), net longwave radiation (LW_{net}), sensible heat fluxes (SHF) and latent heat flux (LHF). Only results in AP are shown.

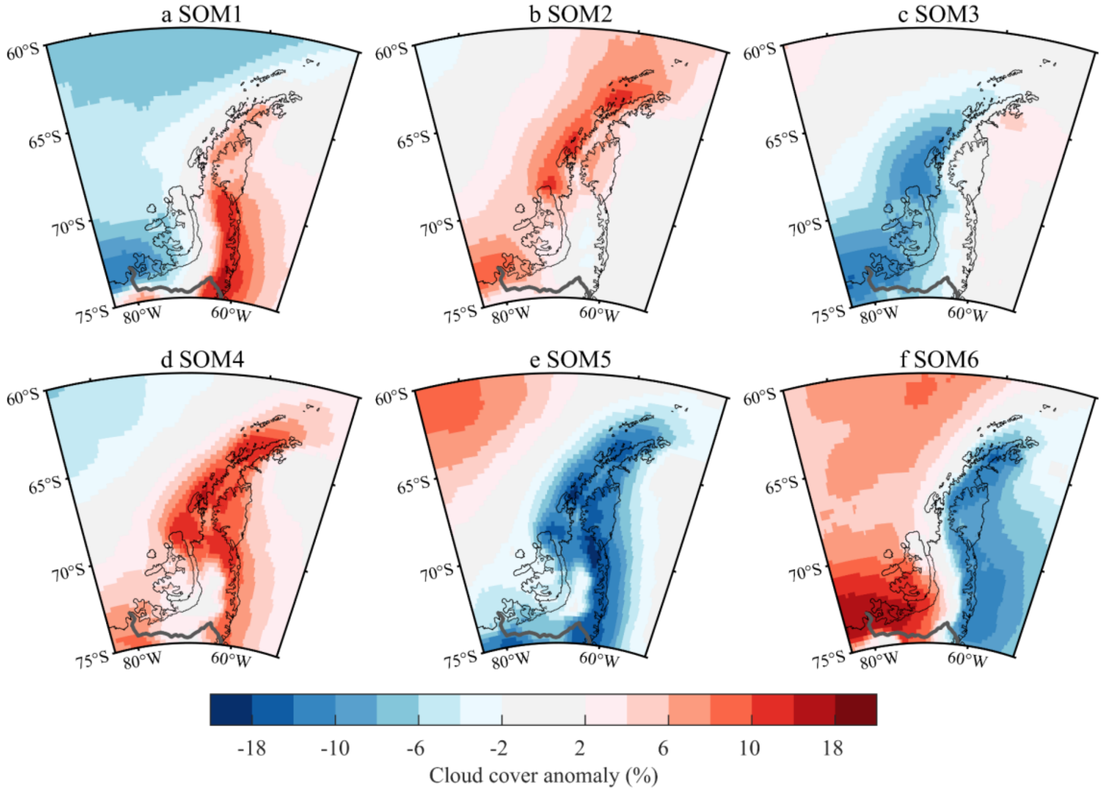

Supplementary Figure 6: Average cloud cover anomalies during each circulation pattern in 1979-2022 NDJF.

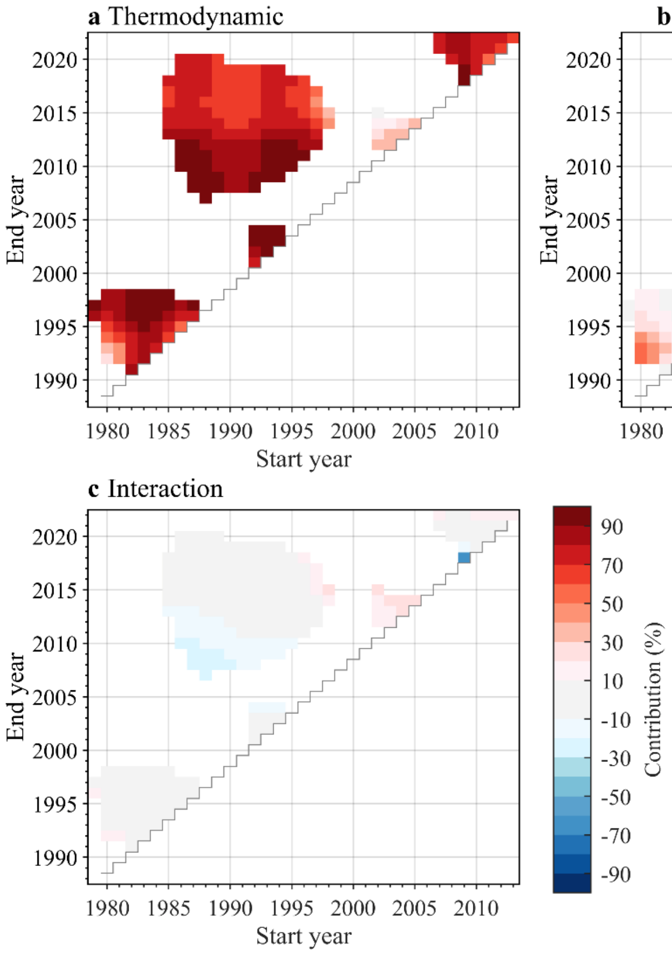

Supplementary Figure 7: Contribution of thermodynamic, dynamic and interaction processes to the melt trend. The surface melt trends during different periods are decomposed into three components, and only the results of trends passing the significance test in Fig. 1c are shown.

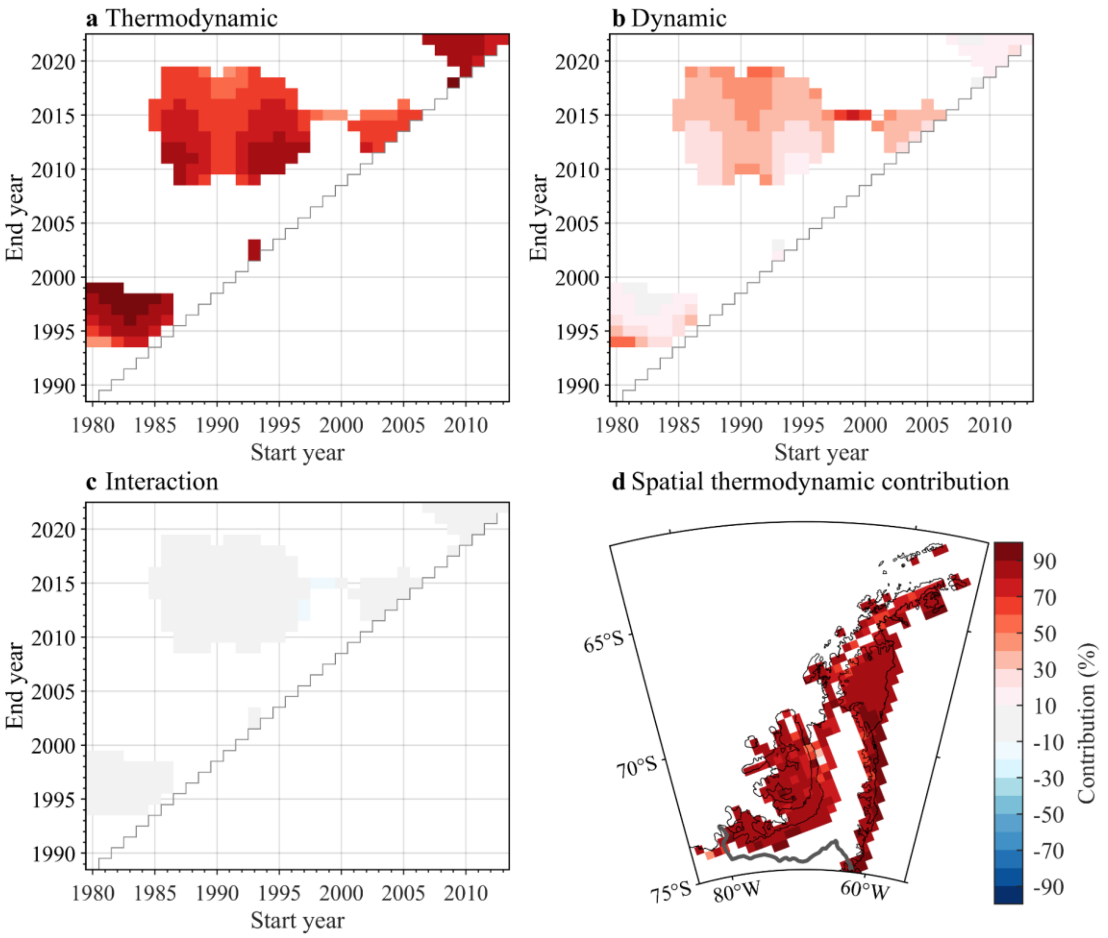

Supplementary Figure 8: Contribution of thermodynamic, dynamic and interaction based on MAR v3.12 outputs. The surface melt trends during different periods are decomposed into three components, and only the results of trends passing the significance test in Supplementary Figure 3 are shown.

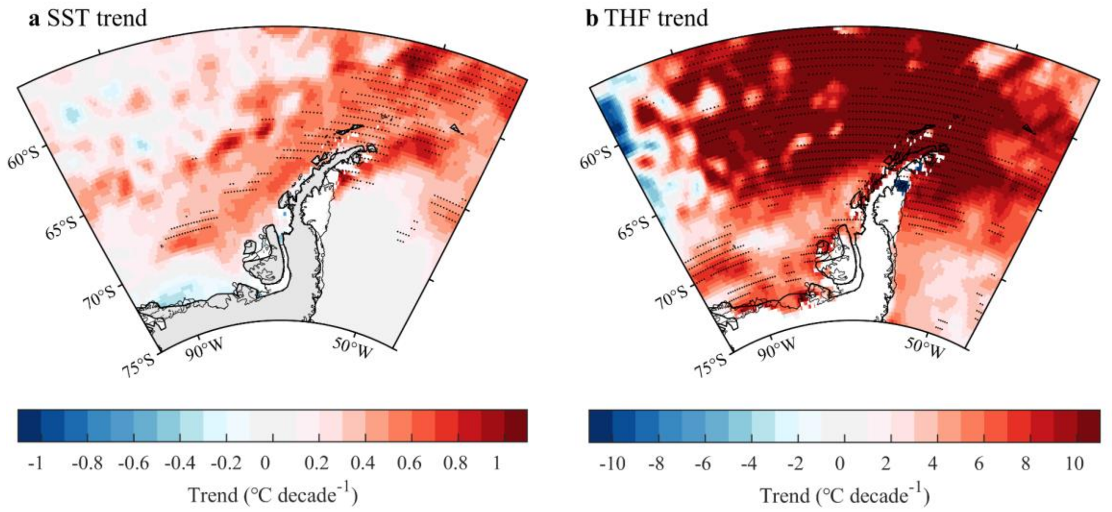

Supplementary Figure 9: Trends of monthly mean NDJF sea surface temperature and turbulent heat flux. **a** Sea surface temperature (SST). **b** Surface turbulent heat flux (THF) since 2009 from ERA5. The black dots represent the 95% significance level t-test. Only results over the ocean are shown.

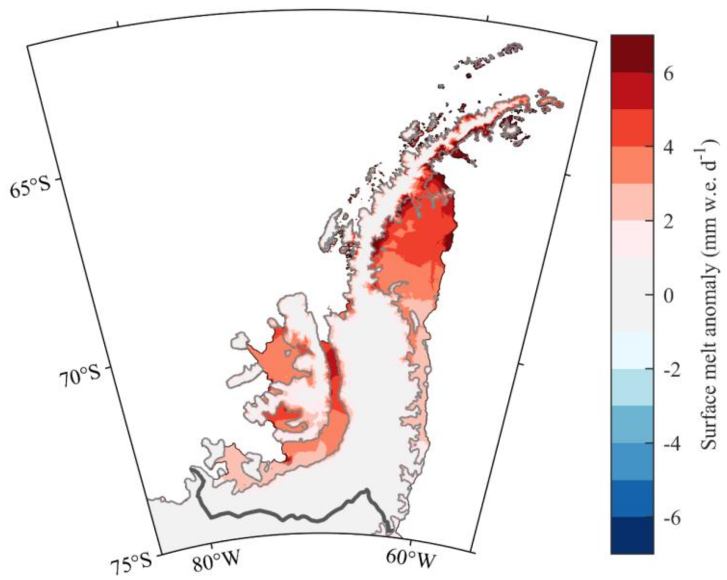

Supplementary Figure 10: Characteristic of AP extreme surface melt. Spatial distribution of averaged extreme surface melt anomalies relative to non-extreme surface melt.

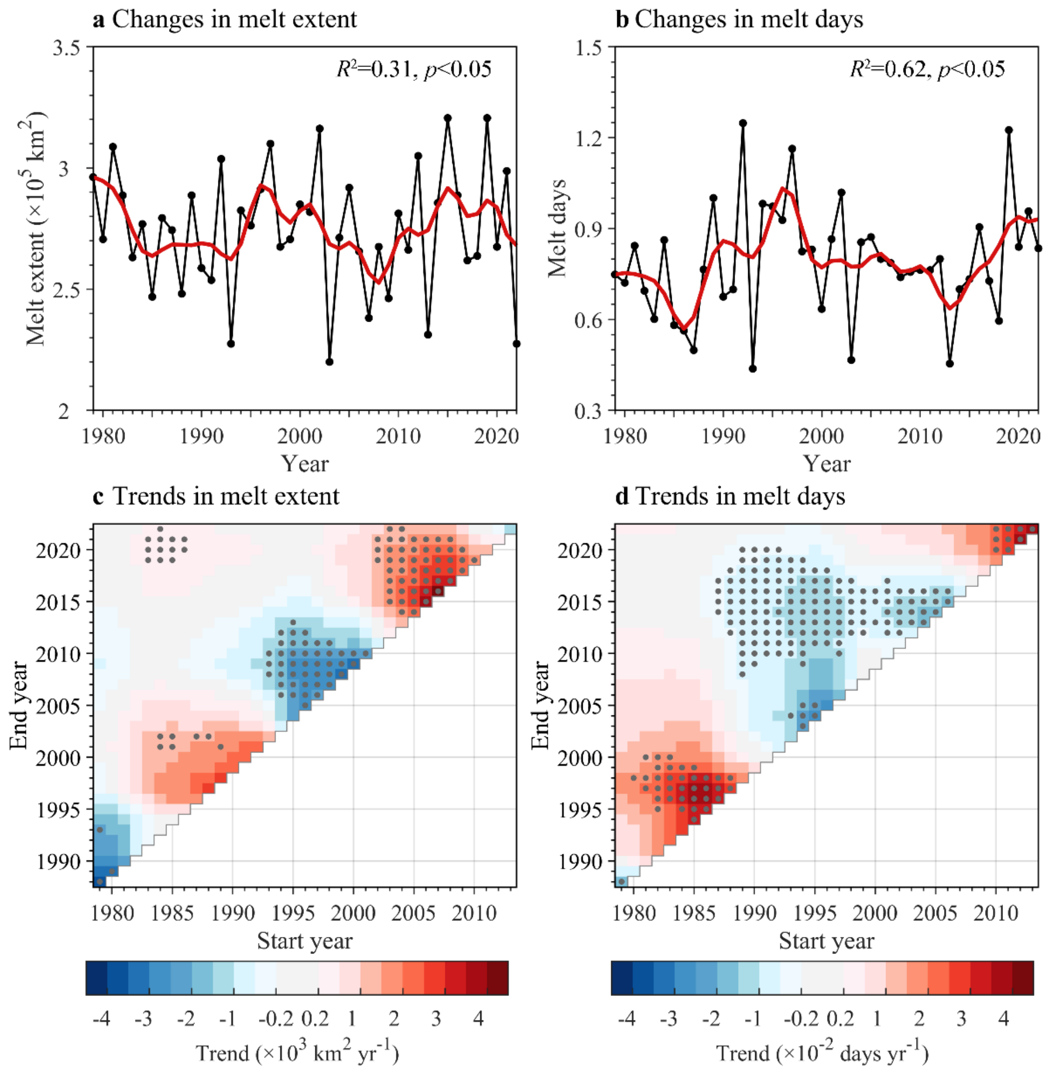

Supplementary Figure 11: Changes and trends in AP NDJF surface melt extent and averaged days from passive microwave satellite. **a, b** Changes in AP NDJF surface melt extent and averaged days. The solid red line represents the results after the five-year low-pass Butterworth filtering. **c, d** Trends during different periods. Linear trends were computed based on the time series represented by red lines in **a** and **b**. Correlations between satellite indices and melt rates are also listed in **a** and **b**. The grey dots in **c** and **d** represent passing the (Hamed-Rao modified) Mann-Kendall significance test of the confidence level of 95%.

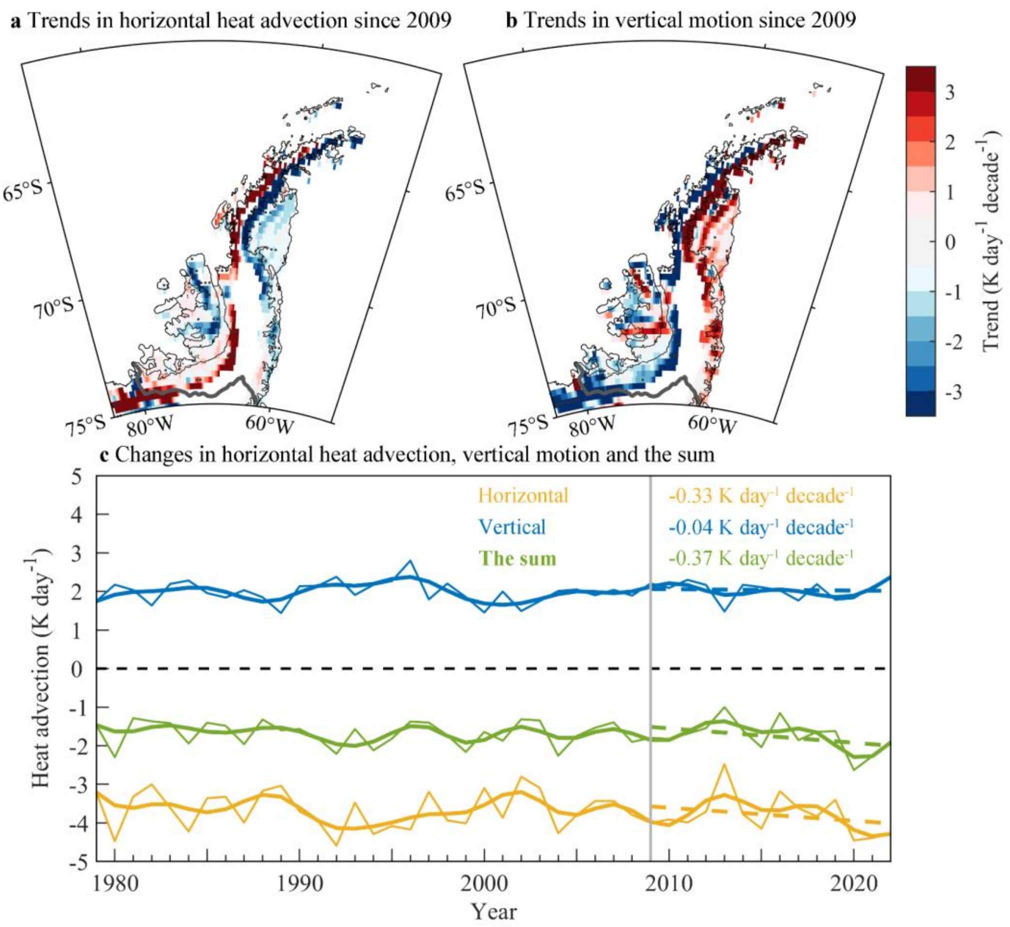

Supplementary Figure 12: Changes in average NDJF dynamical tendency (K day^{-1}) over the Antarctic Peninsula from 1979 to 2022 from ERA5. **a** Trends in average 850 hPa NDJF horizontal heat advection over the AP during 2009-2022. **b** Same as **a**, but for 850 hPa vertical motion (vertical adiabatic warming and vertical advection) over the AP during 2009-2022. **c** Changes in average 850 hPa NDJF horizontal heat advection, vertical motion and their sum over the AP from 1979 to 2022. The bold lines represent the results after the five-year low-pass Butterworth filtering. The regions with surface pressure lower than 850 hPa are masked and not used for computing regional mean. The numbers in **c** indicate the linear trends during 2009-2022 NDJF of regional-average dynamical tendency. All trends in **c** are not statistically significant. The black dots in **a** and **b** represent passing the (Hamed-Rao modified) Mann-Kendall significance test of the confidence level of 95%.

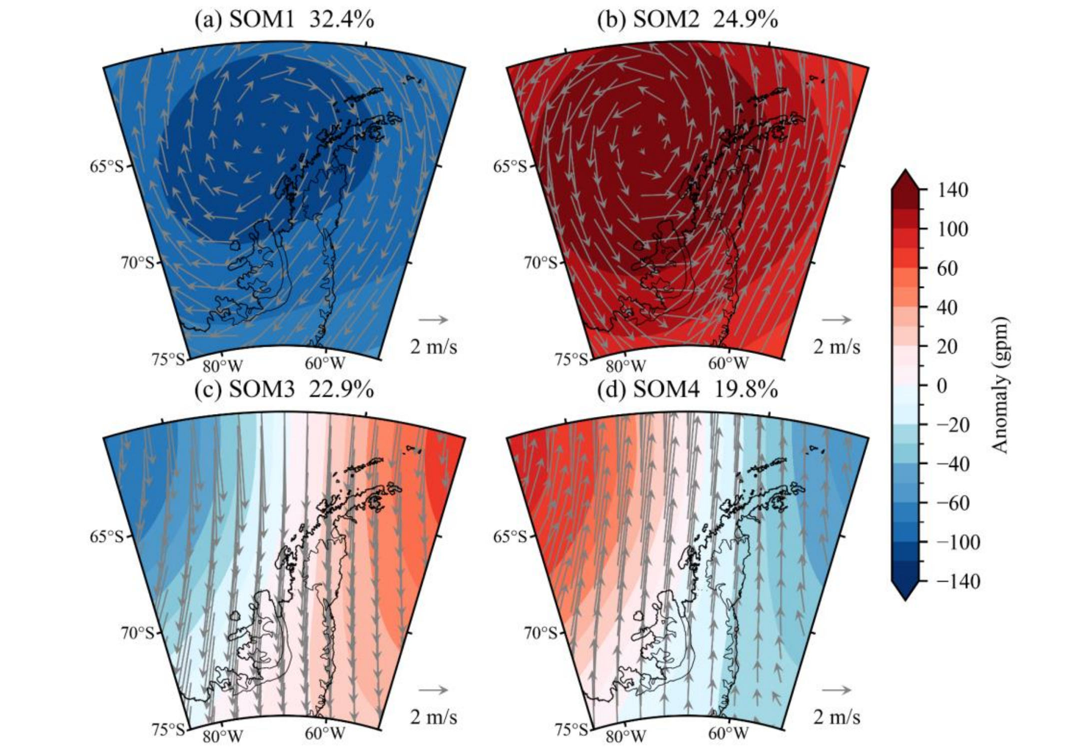

Supplementary Figure 13: Four SOM patterns of daily circulation maps ordered by fractions over the AP in NDJF. In this case, the size of the neural node was set to 2×2.

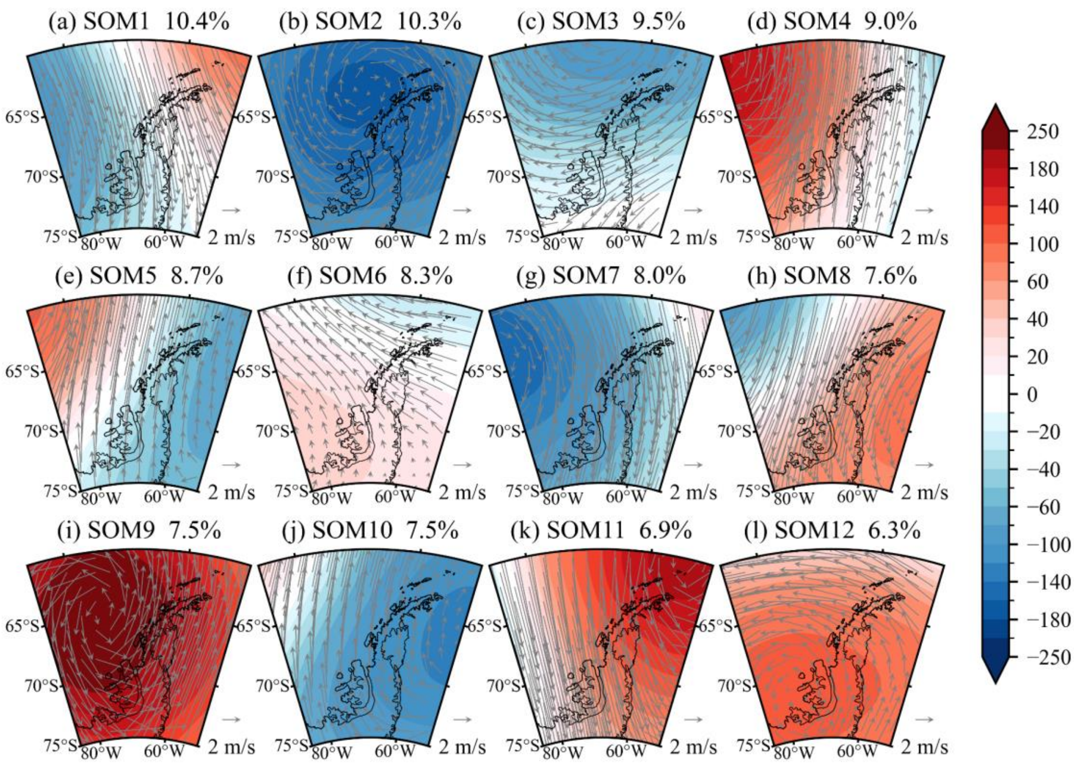

Supplementary Figure 14: Nine SOM patterns of daily circulation maps ordered by fractions over the AP in NDJF. In this case, the size of the neural node was set to 3×4.

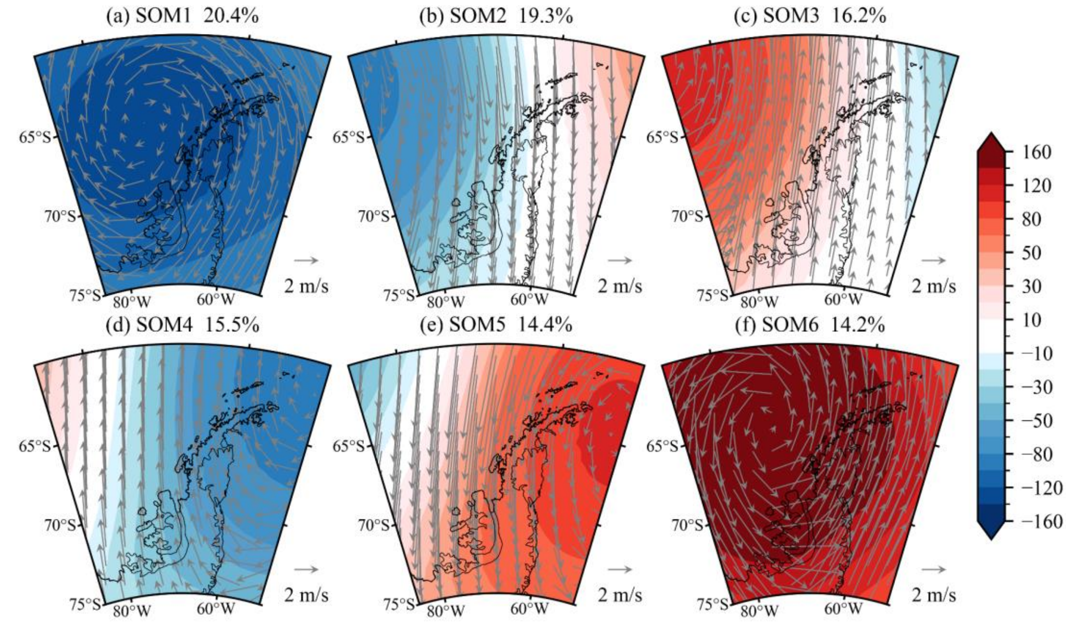

Supplementary Figure 15: SOM patterns of daily circulation maps ordered by fractions over the AP in NDJF. Data comes from MERRA-2. MERRA-2 is available from https://gmao.gsfc.nasa.gov/reanalysis/MERRA-2/. In this case, the size of the neural node was set to 2×3.

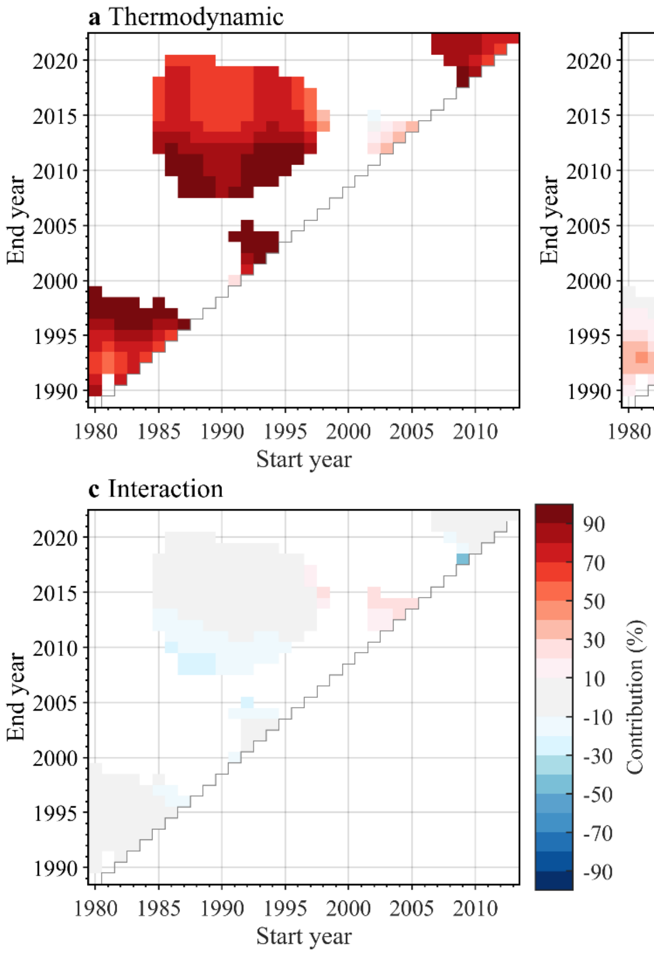

Supplementary Figure 16: Results of contributions decomposition based on the SOM classification of MERRA-2 and surface melt from RACMO2.3p2.

Supplementary Table 1: Settings of the self-organizing maps in this study

Name		Setting
Input		Daily 500 hPa geopotential height anomalies multiplied by the square root of the cosines of the latitude
Node size		2×3
Map		50°–85°W, 60°–75°S
Neighborhood function		Gaussian
Initialization		Linear
Training type		Bath
Initial neighborhood radii	Coarse training	3
	Fine training	2
Final neighborhood radii	Coarse training	1
	Fine training	0.5
Iterations	Coarse training	1000
	Fine training	4000

Supplementary Methods

1. Surface melt extent and days from satellite

AP surface melt extent and days derived from the NASA calibrated enhanced-resolution passive microwave brightness temperatures (Tb) records, including Tb observations from the Scanning Multichannel Microwave Radiometer (SMMR), Special Sensor Microwave Imager (SSM/I) and the Special Sensor Microwave Imager/Sounder (SSMI/S). The National Snow and Ice Data Center (NSIDC, www.nsidc.org) provides the 1979-2023 daily brightness temperature observations with spatial resolution of 25 km × 25 km. We used the Tb from horizontal polarization 18/19 GHz, observed by NIMBUS-7, DMSP SSM/I-F08, DMSP SSM/I-F11, DMSP SSM/I-F13 and DMSP SSMIS-F17. The pixel was defined as the occurrence of surface melting when daily brightness temperature exceeds the average winter (June to August) brightness temperature by 30 K (Zwally and Fiegles, 1995).

2. Dynamical tendency

The horizontal heat advection ($-\mathbf{V}\cdot\nabla T$) and vertical motion (vertical adiabatic warming and vertical advection) are computed based on ERA5 temperature and wind speed from 1979 to 2022 NDJF. The horizontal heat advection can be calculated as follows (Holton and Hakim, 2013):

$$-\mathbf{V} \cdot \nabla T = -\left[u \frac{\partial T}{\partial x} + v \frac{\partial T}{\partial y}\right] \qquad (S1)$$

where, u, v, T are zonal wind, meridional wind (m s^{-1}) and temperature (K) in same pressure level from ERA5. Here, we compute the 850 hPa horizontal heat advection, respectively. The AP regions with mean surface pressure lower than 850 hPa are not shown and not used. The vertical motion is calculated as $\left(\frac{RT}{C_p p} - \frac{\partial T}{\partial p}\right)\omega$, where R, C_p and ω are the gas constant, the specific heat at constant pressure (850 hPa) and the vertical velocity (Pa s^{-1}), respectively. $\frac{\partial T}{\partial p}$ at the 850 hPa level is calculated from the difference of temperature between the 800 hPa and 975 hPa level.

Supplementary References:

Holton, J. R. & Hakim, G. J. In An Introduction to Dynamic Meteorology 5th edn, (eds Holton, J. R. & Hakim, G. J.) 69–70 (Academic Press, 2013).

Zwally, H. & Fiegles, S. Extent and duration of Antarctic surface melting. *Oceanographic Literature Review* **6**, 428 (1995).